JOURNAL OF AIRCRAFT
Vol. 47, No. 5, September–October 2010

Yield Strength and Residual Stress Measurements on Friction-Stir-Welded Aluminum Alloys

H. J. K. Lemmen,* R. C. Alderliesten,† R. R. G. M. Pieters,‡ and R. Benedictus§
Delft University of Technology, 2629 HS Delft, The Netherlands
and
J. A. Pineault¶
Proto Manufacturing Limited, Oldcastle, Ontario N0R 1L0, Canada

DOI: 10.2514/1.C000212

Friction-stir welding is a relatively new joining technology that has great potential for the aerospace industry. To use friction-stir welding to manufacture an airworthy and damage-tolerant structure, the mechanical behavior must be fully understood. This paper presents the experimental results in which the local yield strength and the residual stress profile for friction-stir-welded AA2024-T3, AA7075-T6, and AA6013-T4 were measured. X-ray diffraction was used to measure the residual stresses. The residual stress profiles in all three alloys exhibited high tensile stresses in the center region of the weld. Around the weld the stress levels were reduced to either zero or low-magnitude compressive stresses. Both AA2024-T3 and AA7075-T6 show comparable residual stress profiles, whereas AA6013-T4 exhibits lower-magnitude residual stresses. Digital imaging correlation was used to measure the local yield strength in all three alloys with and without welds. The yield strength profiles obtained with this new technology matched perfectly with the corresponding hardness profiles of the welds. A relation was found between the yield strength profiles and the residual stress profiles, which resulted in understanding of how the appearance of the residual stress profiles is determined by the yield strength profile.

Nomenclature

L	=	longitudinal direction of sheet material
L_0	=	initial gauge length
LT	=	longitudinal transverse direction of sheet material
α	=	friction-stir weld tool angle
σ	=	stress

I. Introduction

FRICTION stir (FS) welding attracts a growing interest from the aerospace industry as a high-potential joining technology for aerospace applications [1–3]. Welding generally offers a reduction in production costs, lead-times, and a decrease in structural weight. FS welding is a solid-state process; this makes it feasible to weld high strength aluminum alloys such as AA2024 and AA7075 with high quality [4,5]. The low process temperatures with maxima below the solidus temperature assure a minimal temperature impact and thus an improved preservation of strength [6]. Furthermore, FS welding is a robust process without emission of hazardous gasses or radiation which requires protection.

However, to use FS welded joints in a damage tolerant aircraft structure, the mechanical behavior must be fully understood. During fatigue experiments on FS welded AA2024-T3 it was observed that the FS weld affect the fatigue crack growth (FCG) rate and direction [7,8]. The authors believe that the FCG behavior is affected by two parameters, the local yield strength and the residual stress profile, because those two parameters affects the size and geometry of the plastic zone in front of the crack tip. To gain more understanding of this relation, three steps must be taken. First the two parameters which affect the FCG behavior, i.e., the local yield strength and the residual stress profiles of the FS welds, must be measured. Second, dedicated FCG tests are required to study the FCG behavior through a FS weld. Third, the effect of the local yield strength and the residual stresses on the principal stress at the crack tip must be analyzed using finite element analysis (FEA).

This paper presents the first step which was performed to obtain the local yield strength and the residual stress profiles of FS welded AA2024-T3, AA7075-T6 and AA6013-T4. FS welding changes the mechanical properties including the yield strength locally, resulting in a complex yield strength profile. Several attempts to measure the local mechanical properties in FS welds have been presented in the literature [2,4,6,9]. However, most approaches were unable to reconstruct the yield strength profile in detail. Microtensile test specimens [10] provide a discrete result and the method is limited by the thickness of the welded material. Furthermore, standard tensile tests provide only average properties of the FS weld including a portion of the parent material. To improve the accuracy and resolution of the yield strength measurement, digital imaging correlation (DIC) software was developed and applied successfully to measure the local strain in a tensile test specimen containing a FS weld. By combining the strain in the images with the measured load, local stress-strain curves were obtained from which the local yield strength was deduced. This approach turned out to be very successful with yield strength profiles for each FS weld as a result.

Residual stresses can be measured using different techniques as described in the literature [11–14]. For this work, the residual stresses in and around the FS welds were measured by Proto Manufacturing, Ltd., using X-ray diffraction. X-ray diffraction gives only residual stresses just below the surface of the specimen, but by performing the measurement at both sides of the FS weld and on specimens with different widths and thickness some understanding is gained about the through thickness behavior of the residual stresses.

Presented as Paper 2008-1937 at the 49th AIAA/ASME/ASCE/AHS/ASC Structures, Structural Dynamics, and Materials Conference, Schaumburg, IL, 7–10 April 2008; received 2 December 2009; revision received 18 March 2010; accepted for publication 20 April 2010.

*Ph.D. Student, Aerospace Structures and Materials Laboratory, Faculty of Aerospace Engineering, P.O. Box 5058; H.J.K.Lemmen@tudelft.nl.

†Assistant Professor, Aerospace Structures and Materials Laboratory, Faculty of Aerospace Engineering, P.O. Box 5058; R.C.Alderliesten@tudelft.nl.

‡Assistant Professor, Aerospace Structures and Materials Laboratory, Faculty of Aerospace Engineering, P.O. Box 5058; R.R.G.M.Pieters@tudelft.nl.

§Professor, Aerospace Structures and Materials Laboratory, Faculty of Aerospace Engineering, P.O. Box 5058; R.Benedictus@tudelft.nl.

¶2175 Solar Crescent; xrdlab@protoxrd.com.

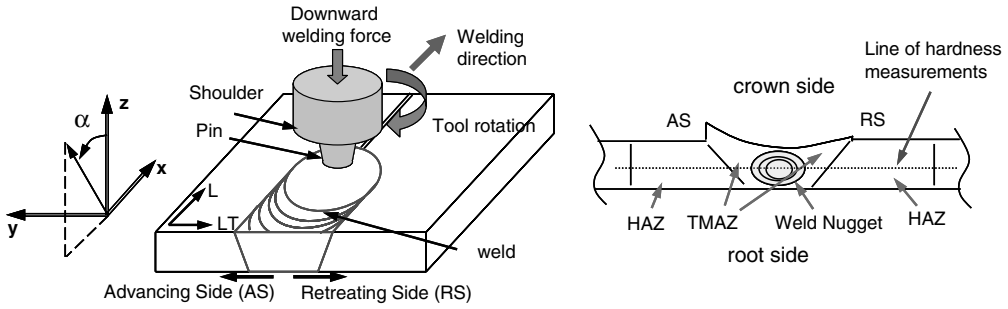

Fig. 1 Characteristics of the FS weld process: a) schematic drawing of weld process with orientations of material and global axes and b) cross section of weld with locations of weld zones and hardness measurements.

II. Experiments

A. Production of the Welds

The welds for this research were produced at EADS in Munich using an ESAB FS weld machine. A tool (Fig. 1a) with a shoulder and pin diameter of 13 and 5 mm, respectively, was used for all three alloys with a tool angle of $\alpha = 2°$. A threaded triflute conical pin was used to weld the three alloys for this research, i.e. AA2024-T3, AA7075-T6 and AA6013-T4 with the process parameters as given in Table 1. In general, three zones can be distinguished in the FS weld (Fig. 1b), the stirred zone or weld nugget, the thermomechanically affected zone (TMAZ), and the heat affected zone (HAZ). All three zones have different thermal and/or mechanical history. Because of the rotation of the FS welding tool in combination with the traverse speed of the specimen, the difference in speed between the tool and the specimen is higher on one side compared with the other; these sides are defined as the advancing side and the retreating side, respectively, (Fig. 1a). Prior to welding, the oxide layer was removed from the edge by a wire brush and cleaned with acetone. The sheets were clamped and a sheet of highly oxidized carbon steel was placed below the specimens to prevent them being welded to the table. All welds were performed parallel to the rolling direction of the aluminum (Fig. 1a), because this is the common orientation of a longitudinal joint in an aircraft fuselage.

Four sheets were welded together with a distance between the welds of 150 and 124 mm. From those sheets, the tensile test specimens perpendicular to the weld were produced and are defined as the long transverse (LT) specimens. The tensile test specimens parallel to the weld, defined as the longitudinal (L) specimens, were produced from sheets containing multiple welds, with an in-between distance of 60 mm.

Between the moment of welding and the mechanical tests was at least a period of four months (except for the hardness measurements which were performed two months after welding) to give the material time to naturally age into its final and stable state.

B. Hardness Measurements

To determine the location and the size of the different zones in the weld, Vickers hardness tests were performed on a cross section of one of the welds. The measurements were performed at the midline of the joint (Fig. 1b). The distance between the indents is 0.2 mm and the applied load was 200 g. The specimens used for the hardness measurements were small enough to release the residual stresses. Therefore, the residual stresses are assumed to have no significant influence on the hardness measurements.

Table 1 FS weld parameters for the three alloys

Alloy	Sheet thickness, mm	Traverse speed, mm/ min	Rotational speed, rpm	Welding force, kN
AA2024-T3	2.5	350	550	19
AA7075-T6	2.0	300	280	18
AA6013-T4	1.8	1000	1500	14

C. Tensile Tests with Digital Image Correlation

To measure the local yield strength in the FS welds, DIC was applied with software developed by the author [9,15–17]. DIC analysis the images taken from a tensile test and translates the deformations in the images into strains (Fig. 2). For the DIC, images were captured during the tensile tests with a CCD camera, using a frequency of 3.75 Hz. Meanwhile, the load applied to the specimen, the time and a trigger signal were recorded simultaneously. The trigger signal was used to synchronize the images with the recorded data from the test machine. After the tests, the applied load was correlated to the strain measured in the images resulting in the local stress-strain curves. From the local stress-strain curves the local yield strength was determined.

The tensile test specimens were designed according to the standard ASTM E8M04. The tensile test specimens were produced from welded and unwelded AA2024-T3, AA7075-T6 and AA6013-T4. The welds were tensile tested in two directions, perpendicular (LT) and parallel (L) to the weld (Fig. 2). To obtain an indication for the scatter in the FS weld process, more than one weld was tested for each alloy. The tensile tests on unwelded material were performed to obtain the parent material properties of the three alloys in both the L and the LT directions. Both DIC and the standard test method, using an extensometer, were used during the tests on parent material to qualify the DIC method. The parent material test specimens were produced from the same batch as the welded specimens.

The tensile test specimens had a width of 12.5 mm and a gauge length of 50 mm. To avoid any influence from the rough weld surface, the upper and lower surfaces of the welds were machined off resulting in small differences in thickness between the various specimens. The geometry of each specimen was measured prior to testing, with a vernier calliper (accuracy: 0.01 mm) and used to calculate the engineering stress. Because of the small width of the specimens, it can be assumed that the residual stresses are released and have no influence on the mechanical properties. This is certainly the case for the LT test specimens, because the residual stresses are oriented perpendicular to the applied load.

The area captured by the camera was approximately 24 by 18 mm, which is not sufficient to capture the entire FS weld. Therefore, the camera was pointed in some specimens 5 to 10 mm away from the weld center to obtain the material properties in a wider region of the weld. Half of the specimens were tested with the crown side facing the camera while the other half were tested with the root side facing the camera to capture the differences due to the wedge shape of the FS weld.

Some difficulties were encountered in aligning the camera perpendicular to the specimen in combination with having the specimen in the center of the image. To solve this, the camera was first perpendicular aligned to the specimen and afterwards the specimen was adjusted in the clamps to get it in the center of the image, resulting in small misalignments of maximal 2 mm with the center of the clamps. Furthermore, the camera was aligned with an angle (β) between the specimen and the image smaller than 1°, because the strains are calculated with respect to the axis of the image and not with respect to the specimen itself (Fig. 2). To enable a good correlation an irregular speckle pattern was airbrushed on the

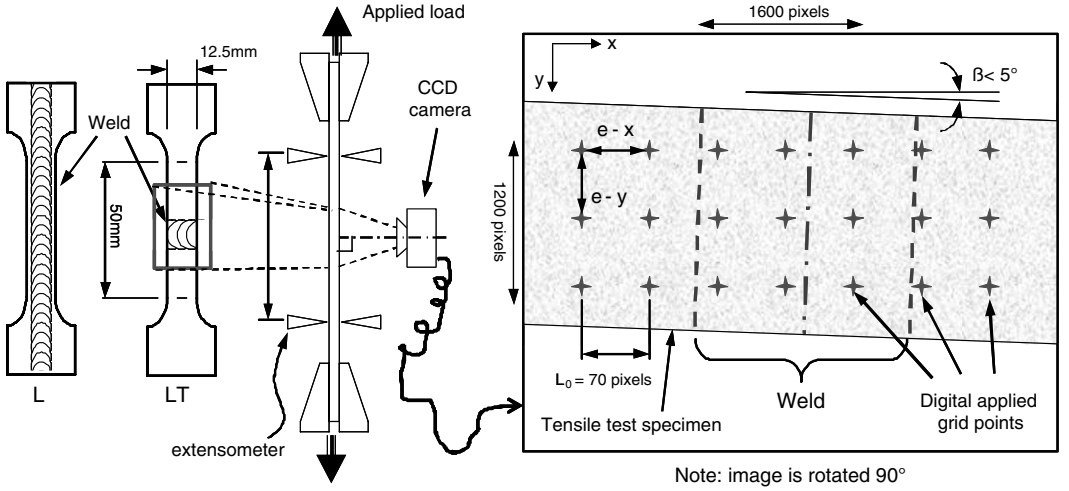

Fig. 2 Schematic overview of tensile test using DIC.

specimen's surfaces. Marker lines were applied, indicating the center of the specimens' gauge section.

The DIC software tool was developed in MATLAB by the author. To enable the strain calculation in the images, a digital grid was defined in the first image of each test to indicate the pixels which had to be correlated in the subsequent images. A distance between the grid points (gauge length L_0) of 70 pixels was used for this research, which corresponds to approximately 1 mm on the specimen. After the coordinates of all the grid points were obtained in the subsequent images, the strains were calculated and combined with the force measured by the load cell from the test machine to obtain the local stress-strain curves. The accuracy of the correlation is at least 0.1 pixels, which is equivalent to 0.14% strain. However, it is possible to obtain an accuracy of up to 0.02 pixels depending on the quality of the test setup and the images.

D. Stress Measurements Using X-Ray Diffraction Techniques

Five specimens were prepared for the residual stress measurements (Table 2). Three specimens contained a weld in the as-welded condition: AA2024-T3, AA7075-T6 and AA6013-T4. The fourth specimen is an untested fatigue initiation specimen prepared for a different research [7]. This specimen is of interest because it was machined to a width of 5 cm, with the FS weld in the center of the specimen. Furthermore, the root of the weld was ground and the crown was machined and ground as preparation for the fatigue initiation test. The fifth specimen contained four different regions each having a different production step applied corresponding to the production steps applied on the tensile specimens and on fatigue initiation specimens. The first region in the specimen is as-welded, the second region was ground at the root side, the third region was ground at the root side and machined at the crown side and the fourth region is the same as the third with an additional 0.1 mm machined off. The different production steps provide information on the influence of these steps on the residual stresses. The measurements were performed by Proto Manufacturing, Ltd.

The X-ray diffraction technique uses the distance between crystallographic planes, i.e. d-spacing, as a strain gage. This method can only be applied to crystalline, polycrystalline and semicrystalline materials [18]. When the material is in tension, the d-spacing increases and when the material is in compression, the d-spacing decreases. Brags law is used for the relation between the wavelength measured by the detector and the d-spacing [19]. The unstressed d-spacing (d_0) is obtained by measuring the d-spacing perpendicular to the specimen's surface, for which the stress is zero at the surface. The strain is calculated by comparing the unstressed d-spacing with the measured d-spacing parallel and perpendicular to the FS weld, giving the longitudinal and tangential residual stresses.

Because the penetration depth of x-ray diffraction is small, it is only possible to obtain the residual stresses at the surface. However, if large differences exist through the thickness of the FS welds; this should become visible by differences between the residual stress profiles measured in region 1, 3 and 4 of specimen five.

To enable a proper x-ray diffraction measurement without any influence from the surface quality, the top surface in the measurement area was removed by electrolytic etching. The electrolytic etch method provided a flat surface without introducing additional residual stresses. The depth of etching was in the order of 0.01 mm.

III. Results

A. Hardness Test Results

Figure 3 shows the hardness profiles in FS welds for three different alloys, i.e. AA2024-T3, AA7075-T6 and AA6013-T4. The influence of FS welding on the hardness depends strongly on the different strengthening system in the three alloys [20]. AA7075-T6 had the highest original hardness, but also the largest decrease in hardness, approximately 50 HV. AA6013-T4 and AA2024-T3 experienced a reduction of 25 HV and 20 HV, respectively. The reduction in hardness for both AA7075-T6 and AA6013-T4 was 24%, whereas AA2024-T3 experienced a reduction of only 14%. In contrast with AA2024-T3 and AA7075-T6, AA6013-T4 had an asymmetric hardness profile.

Table 2 Overview specimens for the residual stress measurements

Specimen number	Alloy	Condition	Size (width × length)
Specimen 1	AA2024-T3	As-welded	20 × 40 cm
Specimen 2	AA7075-T6	As-welded	20 × 40 cm
Specimen 3	AA6013-T4	As-welded	20 × 40 cm
Specimen 4	AA2024-T3	Ground root, machined crown	5 × 60 cm
		Specimen 5	
Region 1	AA2024-T3	As-welded	20 × 40 cm (10 cm per region)
Region 2	AA2024-T3	Ground root side	
Region 3	AA2024-T3	Ground root, machined crown	
Region 4	AA2024-T3	Ground root, machined crown +0.1 mm	

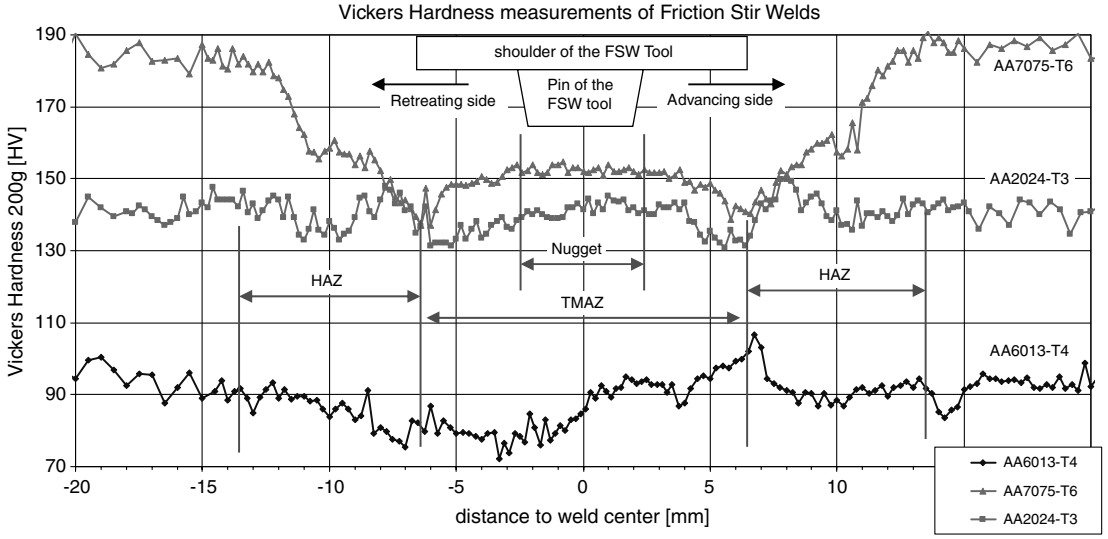

Fig. 3 Hardness profiles of FS welded AA2024-T3, AA7075-T6 and AA6013-T4.

B. Tensile Test Results

Figure 4 shows an example image from a tensile test specimen containing a FS weld in AA2024-T3, which was analyzed using DIC. The local yield strength is visualized in this image by the color scale. The FS weld is clearly distinguished as being perpendicular to the specimen by the regions with low (HAZ/nugget) and high (TMAZ) yield strength. In most of the specimens the yield strength is not constant over the width of the specimen; this is also visible in Fig. 4. This asymmetry of yield strength indicates in-plane bending of the specimen which is caused by the misalignment of the specimens when clamped as described in paragraph IIC. Normally, in-plane bending is not a problem in a tensile test because the effect is averaged out over the gauge length. However, DIC measures the local strains and thus these features become visible. In-plane bending of the specimen causes redistribution of the stress over the cross section and yielding occurs first at the location with the highest stress. However, the local stresses are unknown for these tests because only applied (average) loads were measured. To avoid the influence of in-plane bending and still be able to use the measured data, only the yield strength profiles obtained at the center line of the specimens, close to the neutral axis, are used in this paper.

Figure 5 shows a typical example of the stress-strain curves of FS welded AA2024-T3 extracted from the centerline of a tensile test specimen. The individual stress-strain curves are plotted for clarity with an offset together in one figure with a curve indicating the 0.2% yield strength. The 0.2% yield strength curve is an example of how the curves in Figs. 6–11 are obtained. However, the curves in Figs. 6–11 are plotted with respect to the location in the FS weld instead of the offset of the stress-strain curves in Fig. 5.

The differences in yield strength are clearly distinguished for the specimen with the weld perpendicular to the loading (LT-specimens), while the specimens with the weld parallel to the loading (*L*-specimens) only show a minor difference, which is inherent to the displacement controlled test. In a displacement controlled test, strain is applied and load/stresses are measured, therefore the strain is constant over the cross section of the specimens' gauge section. The stresses will be redistributed locally to comply with the applied strain, but DIC cannot measure these local stresses. As a result, the local stress-strain curves and thus the local yield strengths are equal throughout the weld in the *L*-specimens. Therefore, the results from the *L*-specimens are not further discussed in this paper.

For the results from the LT-specimens, the local yield strength profiles from the root and the crown sides of the welds are plotted separately. All data is plotted according to the sign convention as shown in Fig. 1a, with the advancing side always on the positive side of the *y*-axis.

The parent material tensile tests exhibit the same in-plane bending as the welded specimens. To determine the yield strength for a parent material specimen by DIC, the average value is taken from all local yield strength values obtained for that specimen. The differences between the yield strength obtained with the DIC and with the standard method are on average 2 to 7 MPa for the individual specimens, depending on the experience which was gained during testing. The average yield strength for each set of parent material test specimens obtained by both methods differ less than 4 MPa, as can be seen in Table 3.

The parent material yield strengths in LT direction are presented in Figs. 6–11 by red dotted lines as a reference. No yield strength in the LT direction was obtained for AA7075-T6 therefore the yield strength measured in the *L*-direction was plotted instead.

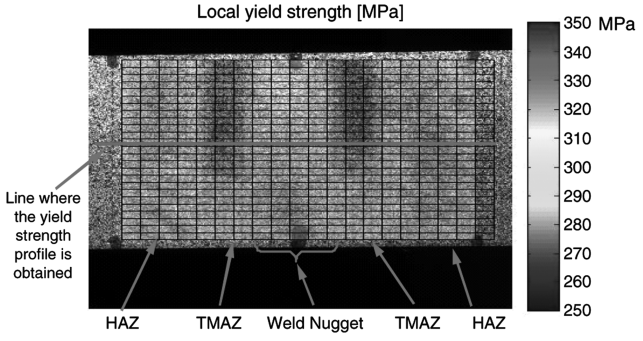

Fig. 4 Typical image of tensile (LT) test specimen, evaluated by DIC; overlay of local yield strength values; FS welded AA2024-T3.

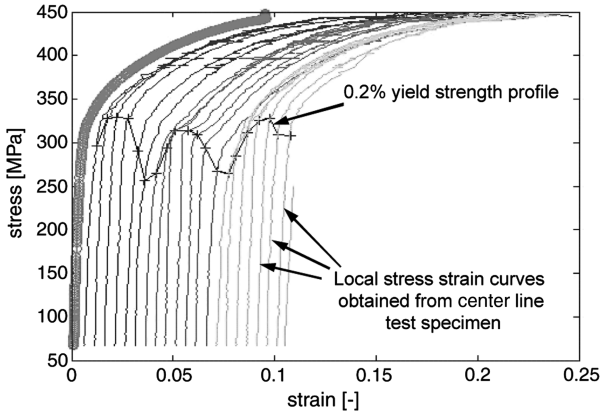

Fig. 5 Typical local stress-strain curves, measured by DIC at the centerline of a tensile test specimen (LT) containing a FS weld in AA2024-T3. The 0.2% yield strength is indicated for each stress-strain curve.

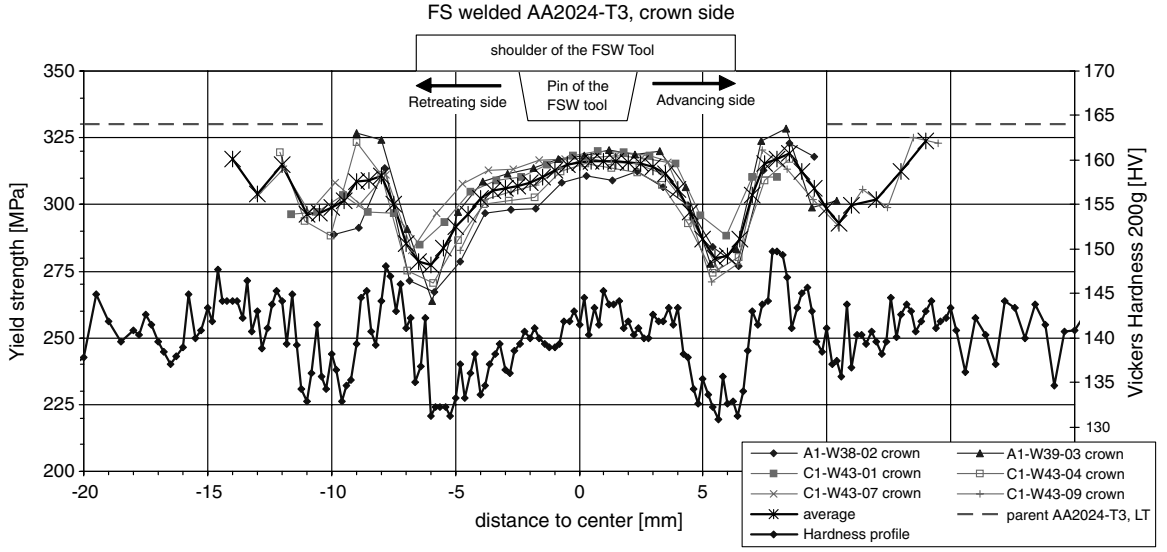

Fig. 6 Yield strength profiles for FS welded AA2024-T3, measured at the crown of the FS weld (left axis) together with the hardness profile from an equivalent FS weld (right axis).

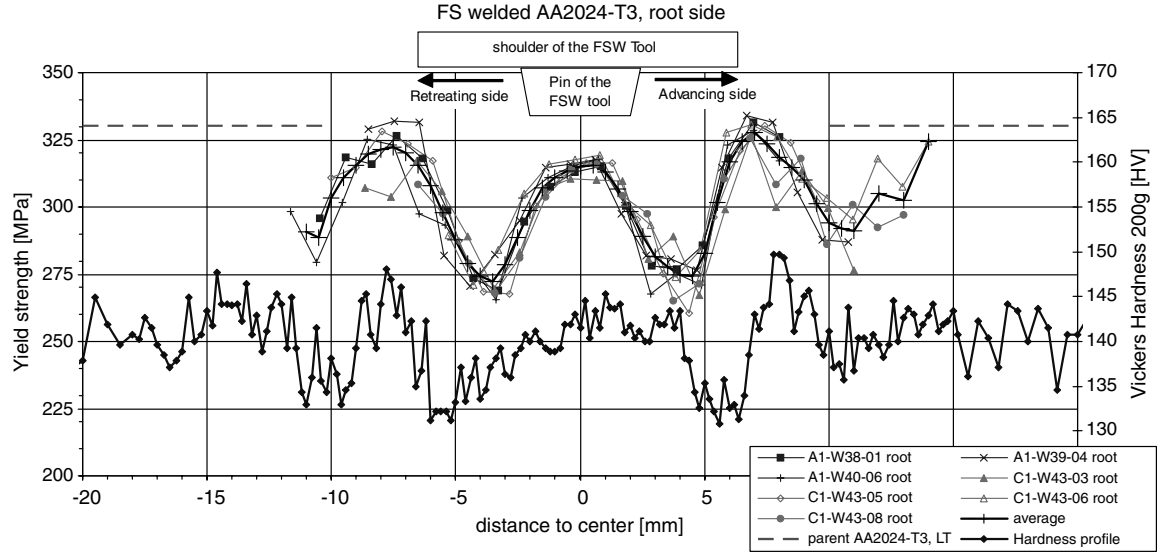

Fig. 7 Yield strength profiles for FS welded AA2024-T3, measured at the root of the FS weld (left axis) together with the hardness profile from an equivalent FS weld (right axis).

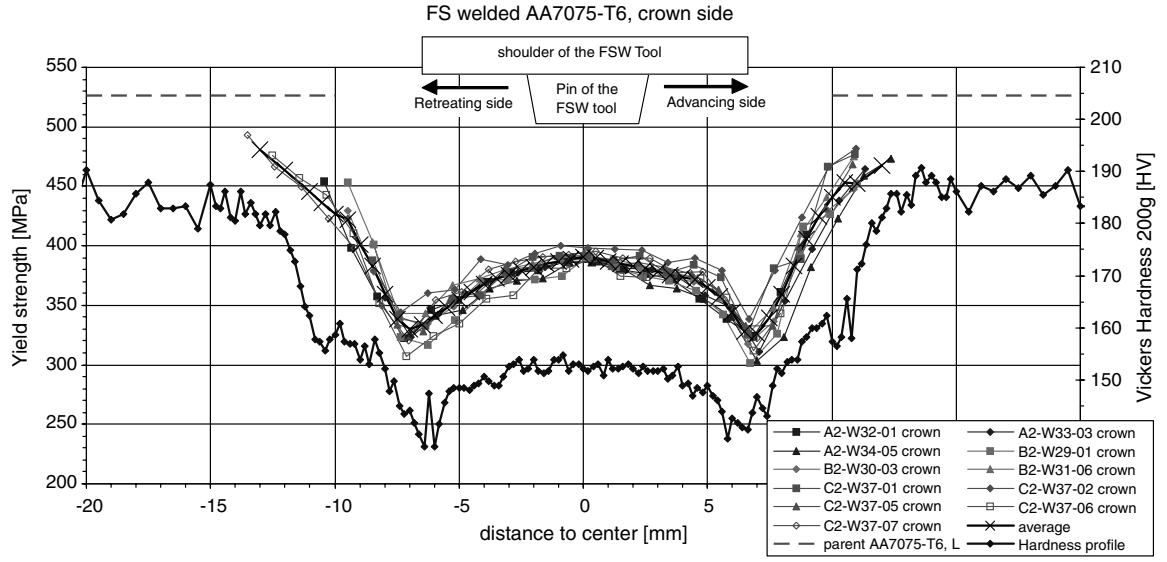

Fig. 8 Yield strength profiles for FS welded AA7075-T6, measured at the crown of the FS weld (left axis) together with the hardness profile from an equivalent FS weld (right axis).

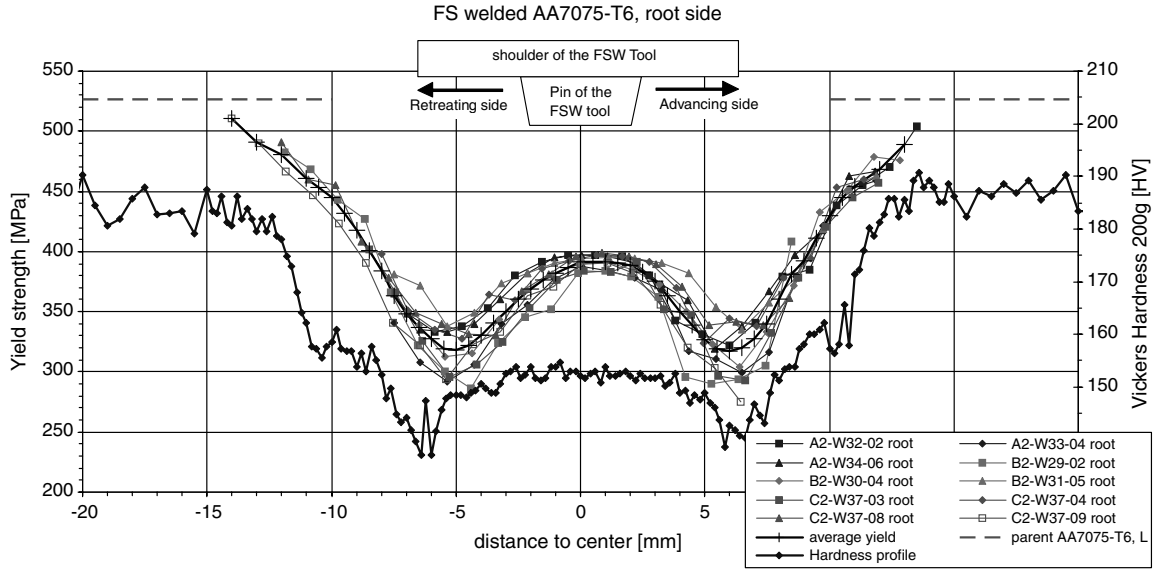

Fig. 9 Yield strength profiles for FS welded AA7075-T6, measured at the root of the FS weld (left axis) together with the hardness profile from an equivalent FS weld (right axis).

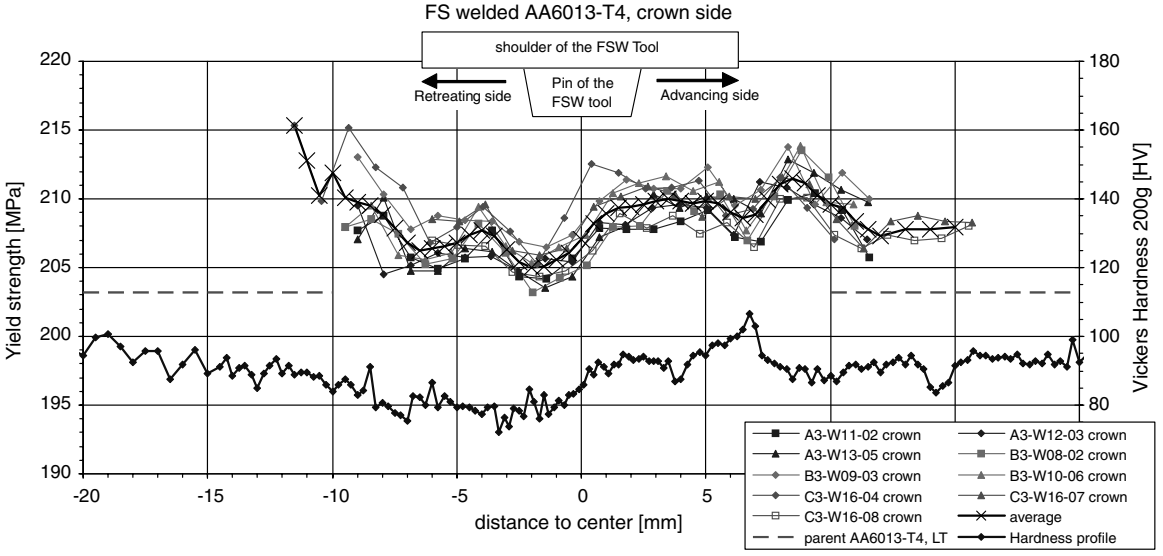

Fig. 10 Yield strength profiles for FS welded AA6013-T4, measured at the crown of the FS weld (left axis) together with the hardness profile from an equivalent FS weld (right axis).

The yield strength profiles are plotted together with the hardness profile of the FS weld. Note that the yield strength is indicated by the scale on the left hand side, while the hardness is indicated by the scale on the right-hand side. Each yield strength profile presents the results from different test specimens.

The yield strength profiles from the crown and root sides of FS welded AA2024-T3 are shown in Figs. 6 and 7 respectively. The yield strength profiles from both sides of the FS weld have the same appearance as the hardness profile. The scatter band is in the order of 10 to 20 MPa. One significant difference between the yield strength profiles from crown and the root sides is the width of the center part which is a result of the typical wedge shape of the FS weld (Fig. 1b). No difference between the yield strength profiles from the crown and root sides can be observed beyond 8 mm from the weld center. An average yield strength profile is calculated and plotted to be used in other figures shown later in this paper.

As mentioned before, the camera was pointed for some tests 5 mm towards either side of the weld center to obtain the yield strength profiles from a larger area. Unfortunately, a shift of 5 mm was not sufficient to capture the properties up to the edge of the FS weld where the weld material properties diminish and the parent material properties become prevalent.

The yield strength profiles of welded AA7075-T6, measured on the crown and the root sides, are shown in Figs. 8 and 9 respectively, together with the hardness profile of the FS weld. As for AA2024-T3, the yield strength profiles of the AA7075-T6 welds have the same appearance as the hardness profile. A difference exists between the yield strength profiles obtained from the crown and root sides of the weld, which corresponds to the wedge shape of the FS weld. The scatter between the different specimens is 10 to 20 MPa, except for the two valleys at 7 mm from the weld center where the scatter has a value of 50 MPa.

The yield strength profiles of welded AA6013-T4 measured on the crown and the root sides of the FS weld are shown in Figs. 10 and 11 respectively together with the hardness profile of the weld. FS welded AA6013-T4 exhibits an asymmetric yield strength and hardness profile. The absolute difference between the peaks and the valleys is small, i.e., 12 MPa. The scatter between the different tests is low, only

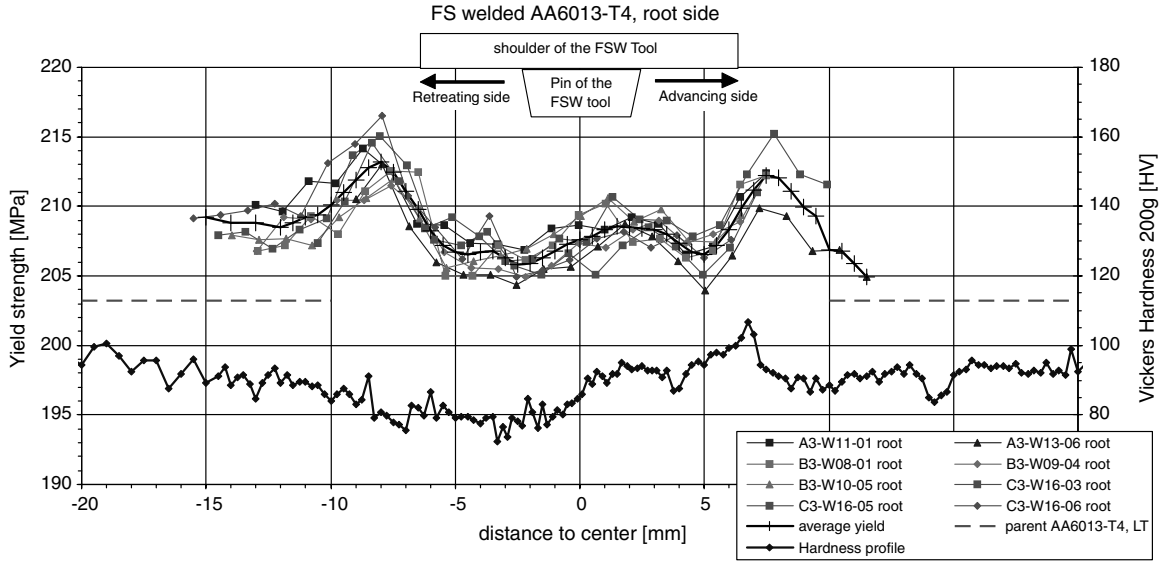

Fig. 11 Yield strength profiles for FS welded AA6013-T4, measured at the root of the FS weld (left axis) together with the hardness profile from an equivalent FS weld (right axis).

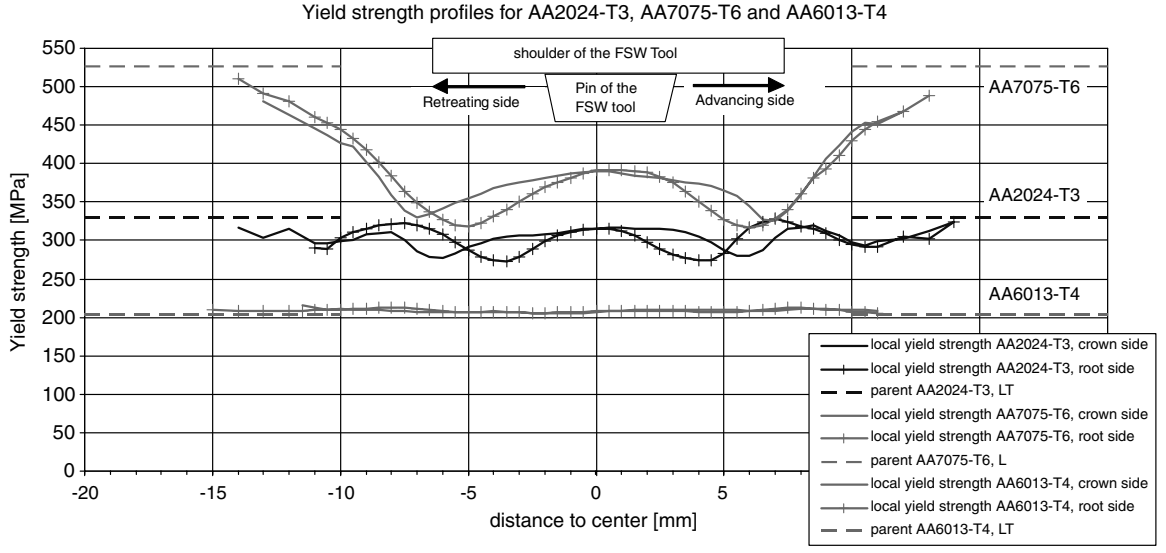

Fig. 12 Yield strength profiles for AA2024-T3, AA7075-T6 and AA6013-T4.

4 MPa. Both the hardness profile and the yield strength profile have a similar appearance. A difference in width is found for the yield strength profile measured on the root and the crown sides of the weld. From the different test results, an average curve is calculated which will be used in subsequent figures.

The average yield strength profiles from the three FS welded alloys are plotted together in Fig. 12. Just as for the hardness profiles shown in Fig. 3, the effect of FS welding on the yield strength is highly dependent on the temper and the strengthening mechanisms of the alloy. Therefore, the reduction of yield strength for AA7075-T6 (artificially aged) is much larger than for AA2024-T3 (naturally aged), whereas AA6013-T4 (soft temper) shows almost no change of yield strength in the FS weld.

Table 3 Parent material yield strength in *L* and LT direction

Method		AA2024-T3	AA7075-T6	AA6013-T4
DIC	*L*	351.6 MPa	526.9 MPa	220.2 MPa
Standard	*L*	352.9 MPa	526.5 MPa	220.7 MPa
DIC	LT	328.5 MPa	——	203.2 MPa
Standard	LT	333.4 MPa	——	202.1 MPa

C. Residual Stress Measurements

The residual stress measurements on specimen 5 indicate that the different surface treatments have a significant influence on the residual stresses at the surface of the specimen. However, little influence of the surface treatments on the residual stress profiles was observed 0.1 mm below the surface (see Fig. 13). Therefore, only the subsurface residual stress measurement results, which are not influenced by any surface treatment, are presented in this paragraph.

Figures 13 and 14 show the residual stress profiles across the weld in the *L* (parallel to the weld) and LT (perpendicular to the weld) direction, respectively, for FS welded AA2024-T3. Both figures show the results from specimen 1 and 5 and different surface treatments (region 1, 2 and 4) (Table 2). The results from both, the crown and the root of the FS weld are plotted, but only the cases which matter.

The residual stress profiles measured in *L* direction show several similarities (Fig. 13), with tensile stresses in a 20 mm wide region in the center of the FS weld. The residual stresses measured at the

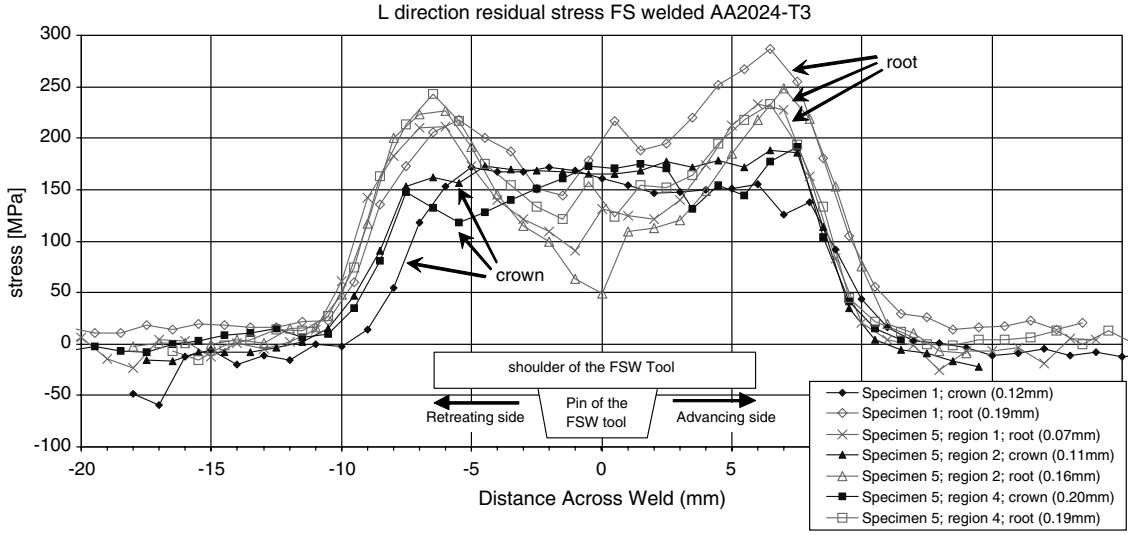

Fig. 13 *L* direction residual stress profiles (parallel to weld) for FS welded AA2024-T3 (specimen 1 and 5).

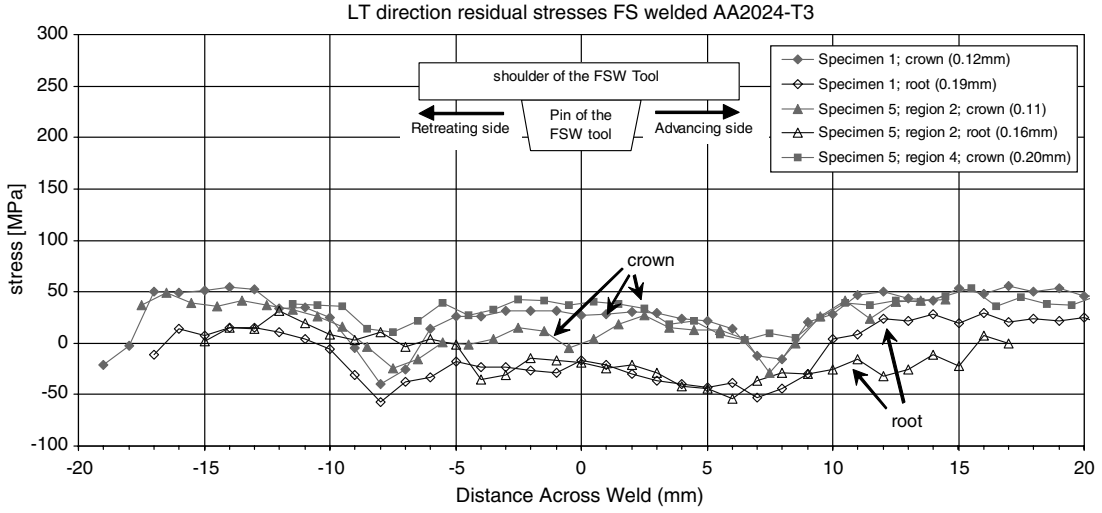

Fig. 14 LT direction residual stress profiles (perpendicular to weld) for FS welded AA2024-T3 (specimen 1 and 5).

crown, rise to a constant level between +120 and +170 MPa, while the residual stresses measured at the root show two peaks at 7 mm on either side of the weld center line. Specimen 1 shows a higher stress peak on the advancing side (positive side) than on the retreating side. Between the two peaks, the residual stresses show different behavior for different specimens, in some it declines to a stress level lower than the residual stress measured at the crown while other specimens show a peak. The width of the region with tensile residual stress is equal for both the crown and the root of the FS weld. The residual stress level outside the FS weld is small in all specimens, which is unexpected because it seams as if no equilibrium exists.

The LT direction residual stress profiles exhibit tensile residual stresses up to +50 MPa outside the weld and two valleys 7 mm from the weld center line were observed (Fig. 14). Between the two valleys, the residual stresses were found to be tensile in some of the specimens and slightly compressive in others, but never higher than the stress levels measured outside the weld. The residual stresses at the root are in general lower in magnitude between the two valleys than the residual stresses at the crown. The two valleys in the residual stress profiles are more easily distinguished at the crown of the FS weld than at the root.

Figure 15 shows the *L*-direction residual stress profiles for specimen 4 together with the residual stress profiles of specimen 1. As can be seen, the residual stress profiles from specimen 4 are equal to the profiles in specimen 1, but shifted 50 MPa downward.

Figure 16 shows the residual stress profiles measured at FS welded AA7075-T6 (specimen 2, in as-welded condition) in both the *L* and LT directions. The residual stress profiles of FS welded AA7075-T6 have a lot in common with the residual stress profiles of FS welded AA2024-T3. Tensile residual stresses in the *L* direction are observed in the region 20 mm from the weld center line. The only difference between the residual stresses on the crown and root sides is the presence of two peaks located 7 mm from the weld center line. The stress levels are comparable to the stress levels found for FS welded AA2024-T3.

For the residual stresses in LT direction on both the crown and root of the FS weld, two valleys at 8 mm from the weld center are present. The residual stresses between these two valleys are higher on the crown than on the root of the FS weld.

Figure 17 shows the residual stress profiles measured in FS welded AA6013-T4 (specimen 3, in as-welded condition). In contrast with AA2024-T3 and AA7075-T6, AA6013-T4 exhibits different residual stress profiles. The magnitude of the *L* direction residual stresses is lower than measured for other two alloys and the two peaks measured at 8 mm from the weld center are sharp. Again, the peaks on the advancing side are higher than on the retreating side of the FS weld. No difference is found between the residual stress profiles measured at the crown and the root of the FS weld. Outside the FS weld, the residual stresses are compressive and fluctuate between 50 and 100 MPa.

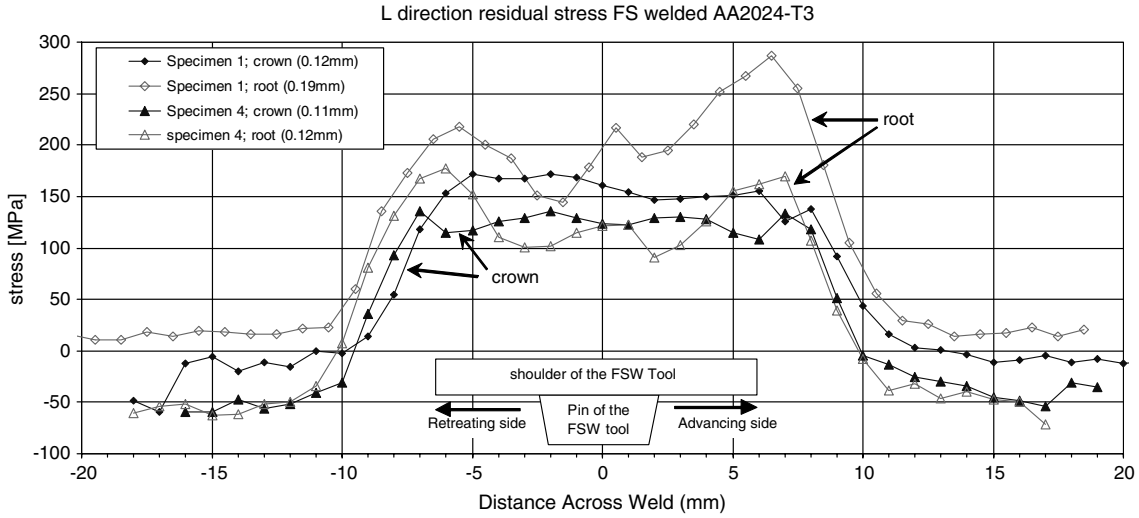

Fig. 15 Different *L* direction residual stress profiles due to different width of specimen 1 and 4, FS welded AA2024-T3 (specimen 1 and 4).

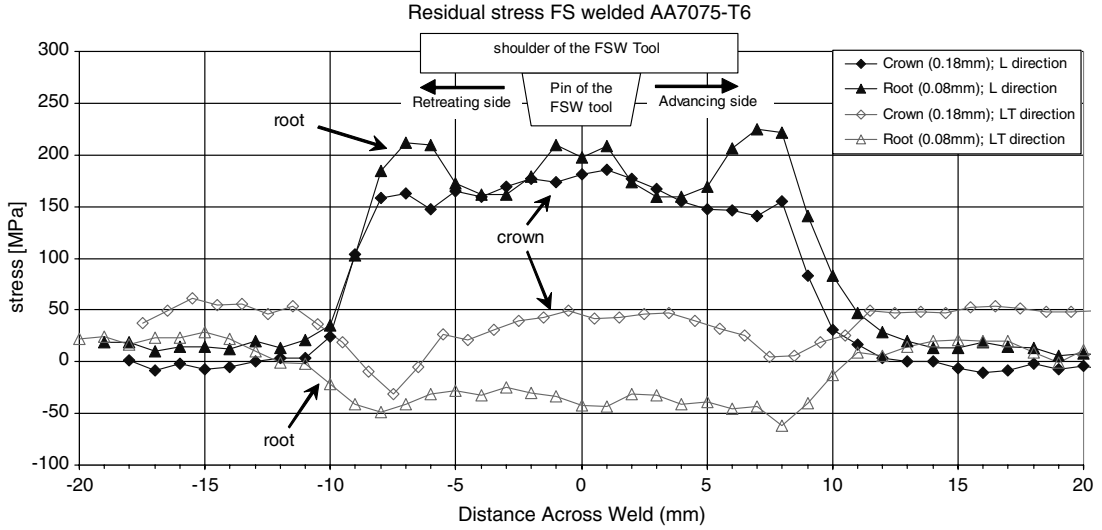

Fig. 16 *L* and LT direction residual stress profiles for FS welded AA7075-T6 (specimen 2).

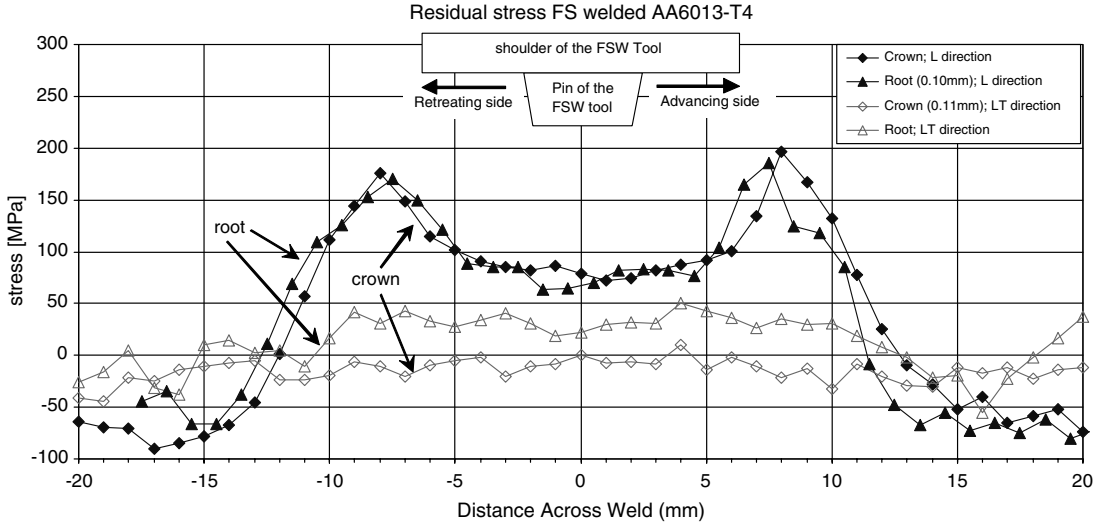

Fig. 17 *L* and LT direction residual stress profile for FS welded AA6013-T4 (specimen 3).

The residual stresses measured in LT direction are constant and slightly below 0 MPa on the crown side of the FS weld whereas on the root side the residual stress increases to a level of +40 MPa in the weld region.

In Fig. 18 the residual stress profiles obtained for the three alloys at the root of the FS weld in *L*-direction, are plotted together (specimen 1, 2 and 3). The residual stress profiles from AA2024-T3 and AA7075-T6 show a similar trend. The peaks and valleys are equal in magnitude and location, except for the peak at the advancing side of AA2024-T3, which is higher. Significantly different is the residual stress profile of AA6013-T4, with its sharp peaks and overall lower magnitudes of residual stresses.

IV. Discussion

A. Yield Strength Profiles

The primary goal of the tensile tests was to measure the local yield strength profiles in a FS weld. However, the results gave much more information than only the yield strength because DIC reveals the complete local stress-strain curve and thus the complete local material behavior is obtained.

The results from the parent material tests (Table 3) show a difference less than 4 MPa between the DIC and the standard measurement method using an extensometer. This is good enough to use the DIC method for the yield strength measurements on FS welded material. It must be stated that the specimens tested first showed larger differences than the specimen tested later due to the gained experience. Because the complexity of the tensile test is increased, more parameters affect the quality of the measurement. Therefore, thorough understanding of the measurement technique is required to obtain meaningful results.

The asymmetry observed in the specimens due to in-plane bending was a major concern until the source was found. Because the nature of in-plane bending, the measurements obtained from the center of the specimen, near the neutral line, are not affected by the bending moment. However, when plasticity occurs this might not be true because nonlinear redistribution of the stresses will occur. However, the method was still assumed to be valid because the deformations up to the yield strength are dominated by linear elasticity and only a small portion of plasticity. The small scatter in the results from the FS welded specimens shown in Figs. 6–11 validate the assumption.

DIC measures only the strains at the specimen's surface, whereas the test machine measures the overall applied load resulting in an average engineering stress value. Up until yielding the stress is equally distributed because the stiffness is equal throughout the FS weld. Beyond yielding the stresses redistribute in a complex way, especially in the wedge shaped nugget region where through thickness differences occur. Besides, the peaks and valleys of the yield strength profiles measured at the crown and root side are similar (Fig. 12) which indicates that the through thickness effect is small.

The width of the LT test specimens is 12.5 mm which is relatively small. Therefore, it may be assumed that residual stresses are released for the major part and thus have no significant influence on the yield strength measurements. An FE analysis is performed to check whether the bi-axial residual stresses have an influence on the tensile test measurements. Both the yield strength and the residual stress profiles presented in this paper are used to simulate the weld in the FE model [21]. The results from this FE analysis show that the residual stresses which are still present in the tensile specimen have no significant influence on the stress in the specimen during the tensile test. Therefore, it may indeed be assumed that the yield strength measurement is not affected by the residual stresses.

In Figs. 6–11 it is shown that the yield strength profiles for all investigated FS welds match the hardness profiles very well, which was expected because yield strength and hardness are closely related properties. However, the ratio between the yield strength and the hardness is not a constant value through the FS weld because this relation is altered by microstructural changes which occur in the material during FS welding. Still, the absolute peaks and valleys of the yield strength profiles and the hardness profiles match well. Therefore, hardness measurements can be used as a qualitative indication of the material behavior in a FS weld.

The yield strength profiles are a function of several processes during and after welding, which are depending on the location in the FS weld. But the temper and the strengthening systems of the alloy determines how large the reduction of the yield strength will be after welding, and how much it can regain by natural aging.

An alloy with a strengthening system with natural aging capabilities, like AA2024 and AA6013, can regain its original strength. Whereas, an alloy with a strengthening system which has limited natural aging capabilities and therefore requires artificial aging, like AA7075-T6, cannot regain its original strength without a heat treatment.

AA6013-T4 showed a larger yield strength at the advancing side than for the parent material (Fig. 10). The increase in yield strength can be explained by the relatively soft temper of AA6013-T4 which enables the alloy to increase the yield strength above the parent material yield strength. The process temperatures at the advancing side are higher than in the rest of the FS weld, which was apparently enough to enable some precipitation strengthening. A more detailed explanation about the relation between the mechanical properties and the effect of FS welding on the precipitation strengthening and microstructural changes is provided in the literature [20,22–24].

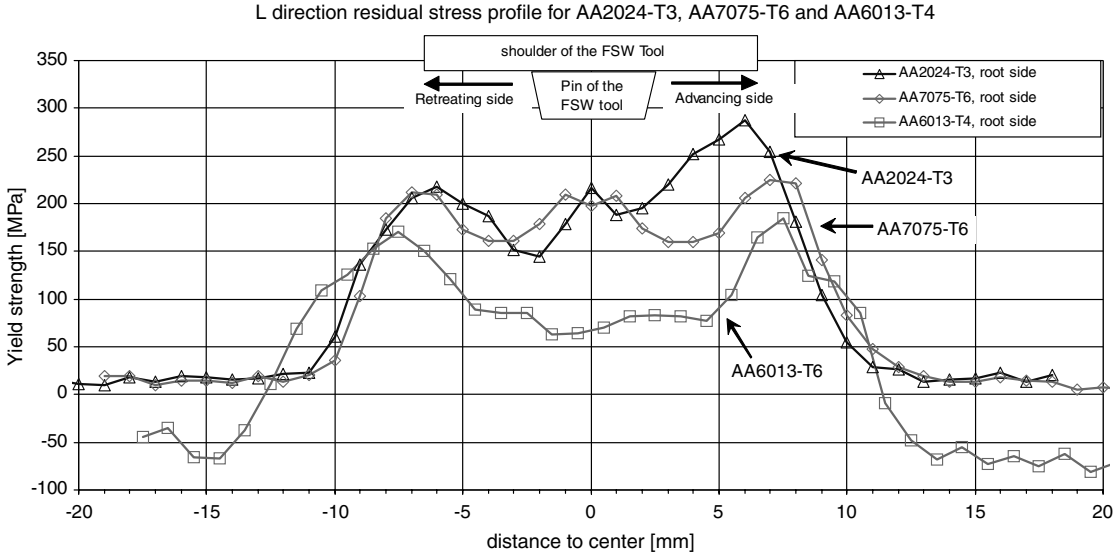

Fig. 18 ***L*** **direction residual stress profiles for AA2024-T3, AA7075-T6 and AA6013-T4.**

Although the weld is highly anisotropic at microscopic level in the nugget/TMAZ, it is assumed that at macroscopic level the anisotropy of the material behavior is limited. The anisotropic behavior can only be a result of the anisotropic grain structure in the nugget/TMAZ, because a change in precipitation hardening affects the material behavior equally in all directions. The influence of the precipitation hardening on the yield strength is in these alloys an order of magnitude higher than the influence of the grain structure. This implies two assumptions to be valid: anisotropy of the yield strength is only present in the nugget/TMAZ and not in the HAZ, because in the latter the grain structure is unchanged and only the precipitation hardening is affected. Secondly; the yield strength in the nugget may be anisotropic due to the grain structure, but the major trend is governed by the change in precipitation hardening. Therefore, small differences may be found in *L* and TL direction for the yield strength profiles in the nugget/TMAZ, but the geometry of these profiles is expected to be equal.

B. Residual Stress Profiles

In general, the residual stress profiles as shown in Figs. 13–17 to comply with the residual stress profiles as previously reported in the literature for different alloys and sheet thicknesses [12–14]. These papers present residual stress profiles with equal geometries. The magnitudes of these stresses differ, but that difference is attributed to the the different process parameters and sheet thickness.

No significant differences between the residual stress profiles measured at the as-welded specimen (specimen 1 and 5, region 1) and the machined specimen (specimen 5, region 4) were found (Figs. 13 and 14). In contrary to the other two alloys, the residual stress profiles from the crown and the root of FS welded AA6013-T4 are equal (Fig. 17), which insinuate that for this alloy the residual stress profiles do not change through thickness.

The small residual stress profiles in *L* direction outside the FS weld for both AA2024-T3 and AA7075-T6 suggest that no equilibrium exists (Fig. 18). Only AA6013-T4 shows compressive residual stresses outside the FS weld to counteract the tensile residual stresses in the FS weld. Several explanations can be put forward for the lack of equilibrium in AA2024-T3 and AA7075-T6; the measurements can be wrong, the residual stresses in the middle of the sheet are lower and counterbalance the tensile residual stresses or the residual stresses are counteracted outside the measurement region. The first explanation is not likely because small scatter was found and several specimens showed the same result. Besides, some results presented in the literature show also residual stress levels of 0 MPa outside the FS weld [14]. The second explanation is less likely because the magnitude of the residual stresses measured at both sides of the FS welds are unchanged for specimen 5, region 4, where material is removed from the surface (Fig. 13). However, this result is not conclusive because the amount of removed material is in the order of 10% of the thickness, which is too small to have a significant effect.

The second explanation is confirmed by the results of specimen 4, because removing the material outside the weld resulted in stress relaxation which shifts the residual stress profile down (Fig. 15). This proves that the material beyond 25 mm from the FS weld center contributes to counterbalance the tensile residual stresses in the FS weld. However, no residual stress measurements were performed beyond 20 mm from the FS weld center.

To understand this behavior, a closer look at the FS welding process where the residual stresses are introduced is required. The residual stress profiles are a summation of the residual stresses due to the thermal cycle in two regions of the FS weld, the nugget and the material around the nugget, which have different load carrying capabilities during welding (Fig. 19). Because the temperatures in the nugget rise to approximately 500°C [25], the nugget has no strength during FS welding, and thus the load carrying capabilities are negligible. Just after FS welding, when the nugget cools down, the load carrying capabilities rise because the material hardens. Cooling down of the nugget also introduces thermal tensile stresses with a magnitude higher than the yield strength present at that moment (left schematic drawing in Fig. 19).

The material surrounding the nugget is capable of carrying thermal loads throughout the whole process, depending on the yield strength, which is a function of temperature. Compressive thermal stresses are introduced in the material around the nugget by heating up during FS welding. Because the compressive thermal stress deforms the material plastically, the reversed situation after cooling down is not the original zero stress state, but a tensile stress field (see middle schematic drawing in Fig. 19). This tensile stress field in the region around the nugget is reduced to counteract the tensile residual stresses which are created in the nugget during cooling down. It depends on the magnitude of the tensile stresses around the nugget whether the residual stresses will be positive, negative, or zero in this region. Off course all the tensile stresses are counterbalanced by the material further away from the FS weld. This theory is not proved by an experiment, but it can explain why no residual stress was measured for AA2024-T3 and AA7075-T6 alongside the nugget.

In contrary to the previous theory, AA6013-T4 shows compressive residual stress alongside the nugget. This could be explained by 3 times higher FS welding speed used for AA6013-T4 (Table 1). A higher welding speed results in lower temperatures [25] and the heat has less time to distribute over a wider region before the nugget starts to harden. Therefore the compressive stresses in the region around the nugget are much smaller, resulting in almost no tensile stresses after cooling down. For the nugget region nothing is changed and thus high tensile stresses will appear in this region. However, these tensile stresses can now be counterbalanced by the material surrounding the nugget because of the lack of tensile stresses in that region.

C. Yield Strength Versus Residual Stress Profiles

To visualize the relationship between the residual stress profile and the yield strength profile, both are plotted for the three alloys in Fig. 20 (crown) and Fig. 21 (root). These two figures show that the center plateau of the residual stress profiles and the yield strength profiles from AA2024-T3 and AA7075-T6 exhibit some similarities, especially at the root side. This is explained by the following mechanism. The residual stresses in the nugget are formed during the cooling down phase of the welding process,

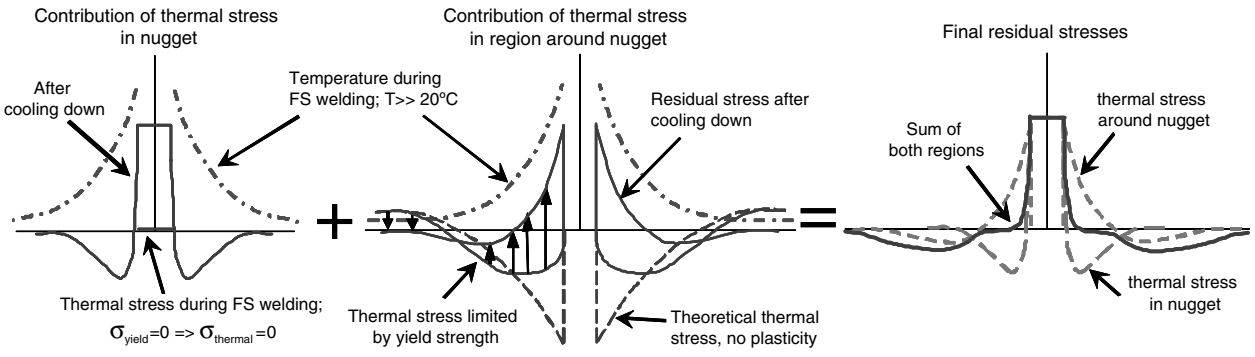

Fig. 19 Schematic overview of the contribution of two regions, the nugget and the region around the nugget, to the residual stress profiles.

because of temperature differences inside and outside the weld. In the same phase the yield strength increases due to the inverse relation between the temperature and the yield strength. The residual stress cannot be larger than the yield strength, because strains larger than the yield strain result in plastic deformation instead of residual stresses. When the material cools down, the yield strength increases and the residual stresses are formed, but are limited by the temporary yield strength. Therefore, the center plateau of the residual stress profile exhibits the geometry of the yield strength profile immediately after the cool down phase.

The residual stress profiles are 50 to 200 MPa below the yield strength profiles, which is attributed to the natural aging process after welding. Natural aging after welding has been shown by hardness measurements and is presented in the literature for AA7075-T651 [26]. In that research, an increase of 30 HV was observed during the first months after welding. Compared with the results in this research, this is approximately 75% of the gab between the residual stress and yield strength profiles (Figs. 20 and 21). Natural aging has two effects; the residual stresses diminish, because diffusion and precipitation leads to stress relaxation, and the yield strength increases. The gap between the yield strength and residual stress profiles is created by both effects.

The influence of the yield strength on the residual stress profile and the process of natural aging is illustrated in Fig. 22. This figure presents the yield strength profile immediately after welding for AA7075-T6 (educated guess based upon the results presented in the literature [26] together with the residual stress profile. The figure shows how the yield strength determines the shape of the center region of the residual stress profile. Because the nugget is wedge shaped, the region with low yield strength is wider at the crown than at the root side, and thus wider than the region with tensile residual stresses at the crown, and visa versa at the root side.

One implication of this theory is that softening of the alloy during welding can be exploited as to avoid the generation of large magnitude residual stresses. For instance, the large reduction of yield strength in FS welded AA7075-T6 resulted in limited magnitudes of residual stresses which are comparable to the residual stresses in AA2024-T3. If AA7075-T6 had the same absolute reduction of yield strength as AA2024-T3, then the residual stresses could have been 200 MPa higher, because the yield strength of parent AA7075-T6 is 200 MPa higher than for parent AA2024-T3.

D. Contribution of this Research

As was stated in the introduction, the research presented in this paper is part of a broader investigation into the fatigue behavior of FS welded joints. The next paragraph describes how the results presented here contributed to this broader research.

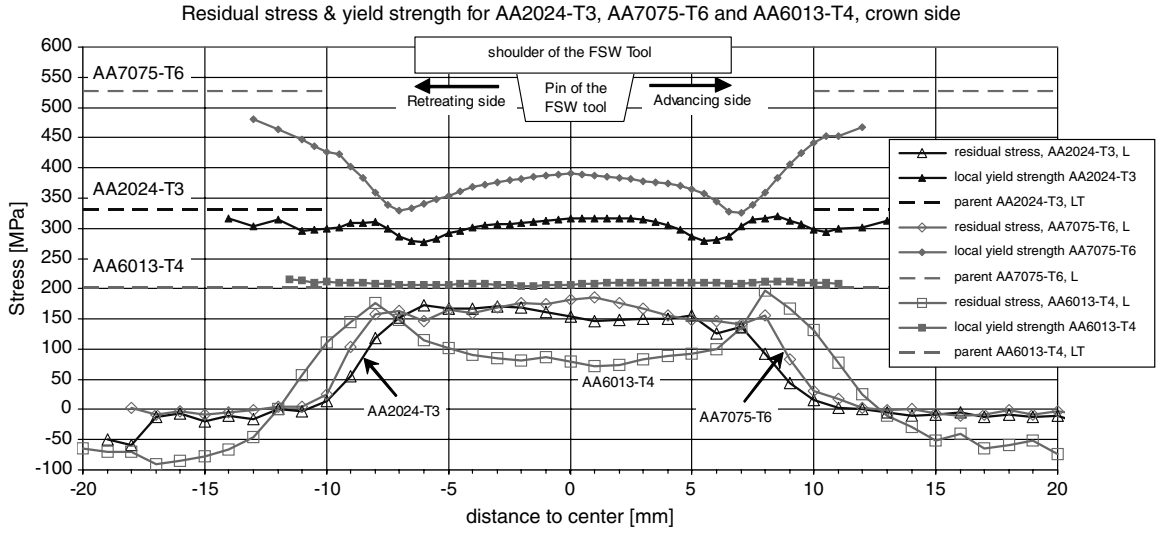

Fig. 20 Residual stress profiles and local yield strength, measured on the crown side, of AA2024-T3, AA7075-T6 and AA6013-T4.

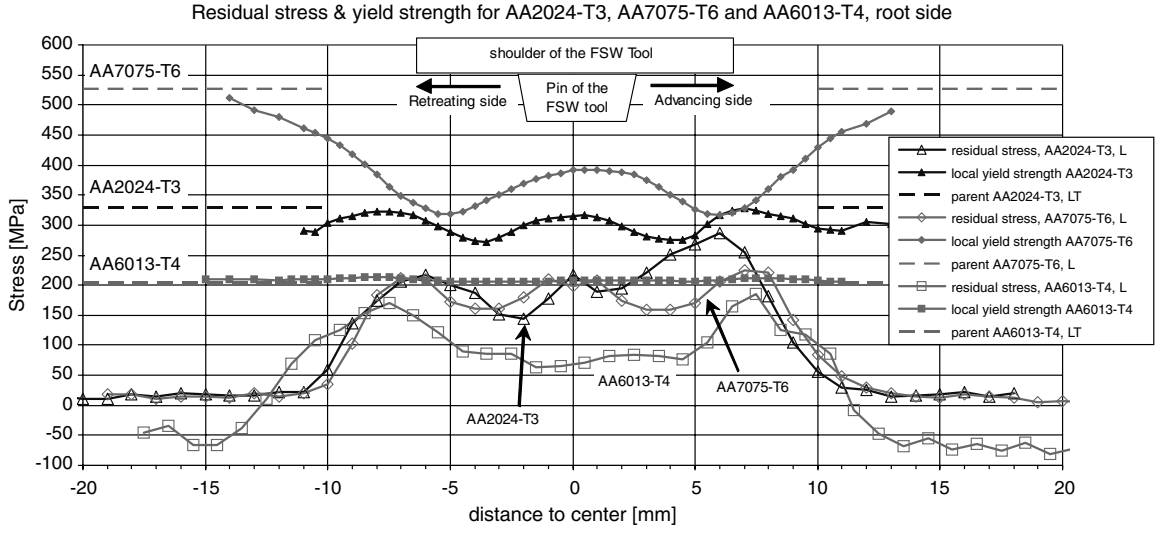

Fig. 21 Residual stress profiles and local yield strength, measured on the root side, of AA2024-T3, AA7075-T6 and AA6013-T4.

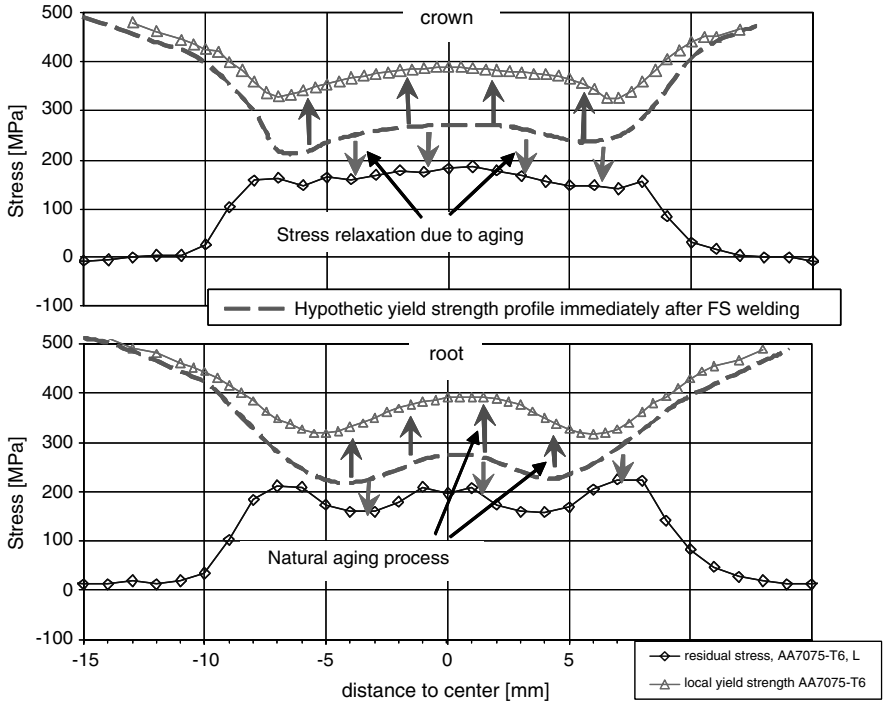

Fig. 22 Influence of the yield strength profiles on the residual stress field for AA7075-T6. Upper: crown, lower: root. Geometry of the center part residual stress profile is determined by the yield strength profile present immediately after FS welding.

The yield strength profiles presented in this paper are unique and ready to be used as input parameters for other research on, or numerical analysis of FS welds. To model the mechanical behavior of a FS weld, for instance by FEA, these yield strength profiles are valuable. Besides, this paper shows that it is possible by using DIC to obtain accurately the detailed mechanical properties of FS welded joints. This paper was limited to the yield strength only, but several other mechanical properties exist which can be extracted from the local stress-strain curves. The experience with the DIC method gained in this research is valuable for other experiments [15], for instance the detailed study of the FCG behavior in and around a FS weld. Moreover, by using two cameras, three-dimensional measurements can be performed on complex shaped specimens, indicating hot spots, or measure the mechanical response of a structural item.

V. Conclusions

The measured yield strength profiles were found to mirror the hardness profiles for all three FS welded alloys, i.e. AA2024-T3, AA7075-T6 and AA6013-T4. However, the ratio between the yield strength and the hardness is not constant throughout the entire profile. The hardness measurements therefore represent a good qualitative indication of the local material properties in a FS weld, but do not represent a quantitative method to measure the local yield strength properties directly.

The residual stress profiles were successfully measured using X-ray diffraction for all three FS welded alloys.

Combining the residual stress profiles and yield strength profiles, it was found that the center region of the residual stress profiles are determined by the yield strength profiles present at the moment the residual stresses were introduced. Therefore the residual stress profiles show the history of the yield strength profiles before the material had time to naturally age. Natural aging causes the yield strength to increase after welding, whereas the residual stress profile is unchanged, which explains why the yield strength profiles are 50 to 200 MPa above the residual stress profiles.

Digital image correlation is an excellent method to measure local material properties. Because DIC is a noncontact measurement technique it has a large degree of freedom.

References

[1] Braun, R., Baillas, G., Donne, C. D., and Staniek, G., "Characterization of Mechanical Properties and Corrosion Performance of Friction Stir Welded AA6013 Sheet," *EUROMAT 99, Biannual Meeting of the Federation of European Materials Societies (FEMS)*, 2000, p. 6.

[2] Bolser, D., Talwar, R., and Lederich, R., "Mechanical and Corrosion Properties of Friction Stir Welded 7050-T7451 Aluminium Alloy," *Welding in the World Soudage dans le Monde*, Vol. 49, Nos. 3–4, 2005, pp. 27–33.

[3] Pacchione, M., Werner, S., and Ohrloff, N., "Design Principles for Damage Tolerant Butt Welded Joints for Application in the Pressurized Fuselage," 24th International Committee on Aeronautical Fatigue Conference, Napels, Italy, 2007.

[4] Cavaliere, P., Cerri, E., and Squillace, A., "Mechanical Response of 2024-7075 Aluminium Alloys Joined by Friction Stir Welding," *Journal of Material Science and Technology (Sofia)*, Vol. 40, No. 14, 2005, pp. 3669–3676.

[5] Donne, C. D., and Baillas, G., "Fatigue and Fracture Performance of Friction Stir Welded 2024-T3 Joints," *Proceedings of the European Conference on Spacecraft Structures, Materials and Mechanical Testing*, Braunschweig, Germany, pp. 309–314.

[6] Biallas, G., Donne, C. D., and Juricic, C., "Monotonic and Cyclic Strength of Friction Stir Welded Aluminium Joints," *Proceedings of Euromat 2000*, Vol. 1, Elsevier, New York, 2000, pp. 115–120.

[7] Lemmen, H. J. K., Alderliesten, R. C., Homan, J. J., and Benedictus, R., "Fatigue Crack Initiation Behavior of Friction Stir Welded Joints in Aluminium Alloy," International Committee on Aeronautical Fatigue Conference, Napels, Italy, 2007.

[8] Lemmen, H. J. K., Alderliesten, R. C., Homan, J. J., and Benedictus, R., "The Influence of Residual Stresses in Friction Stir Welded Joints on the Fatigue Crack Growth Properties," *Computational and Experimental Analysis of Damage Materials*, edited by D. G. Pavlou, Transworld Research Network, Kerala, India, 2007, p. 127–144.

[9] Hector, L. G. Jr., Yen-Lung Chen, Sumit Agarwal, and Briant, C. L., "Friction Stir Processed AA5182-O and AA6111-T4 Aluminium Alloys. Part 2: Tensile Properties and Strain Field Evolution," *Journal of Materials Engineering and Performance*, Vol. 16, No. 4, 2007, pp. 404–417.
doi:10.1007/s11665-007-9060-0

[10] von Strombeck, A., Dos Santos, J. F., Torster, F., Laureano, P., and Kocak, M., "Fracture toughness behavior of FSW joints on aluminium alloys," First International Symposium on Friction Stir Welding, Thousands Oaks, CA, 1999.

[11] Fratini, L., and Zuccarello, B., "An Analysis of Through-Thickness Residual Stresses in Aluminium FSW Butt Joints," *International Journal of Machine Tools and Manufacture*, Vol. 46, No. 6, May 2006, pp. 611–619. doi:10.1016/j.ijmachtools.2005.07.013

[12] Oostkamp, L. D., Webster, P. J., Browne, P. A., Vaughan, G. B. M., and Withers, P. J., "Residual Stress Field in a Friction Stir Welded Aluminium Extrusion," *Materials Science Forum*, Vols. 347–349, pp. 678–683.

[13] James, M. N., Hughes, D. J., Hattingh, D. G., Bradley, G. R., Mills, G., and Webster, P. J., "Synchrotron Diffraction Measurement of Residual Stresses in Friction Stir Welded 5358-H321 Aluminium Butt Joints and Their Modification by Fatigue Cycling," *Fatigue and Fracture of Engineering Materials and Structures*, Vol. 27, No. 3, March 2004, pp. 187–202. doi:10.1111/j.1460-2695.2004.00736.x

[14] Staron, P., Kocak, M., Williams, S., and Wescott, A., "Residual Stress in Friction Stir Welded Al Sheets," *Physica B: Condensed Matter*, Vol. 350, Nos. 1–3.1, 2004, pp. e491–e493.

[15] Lemmen, H. J. K., Alderliesten, R. C., Benedictus, R., Hofstede, J. C. J., and Rodi, R., "The Power of Digital Image Correlation for Detailed Elastic-Plastic Strain Measurements," *Engineering Mechanics, Structures, Engineering Geology (EMESEG '08)*, edited by M.-K. Nikolinakou, G. Tsekouras, V. Gekas, and D. Pavlou, WSEAS Press, Heraklion, Greece, 2008, pp. 73–89.

[16] Hung, P.-C., and Voloshin, A. S., "In-Plane Strain Measurement by Digital Image Correlation," *Journal of the Brazilian Society of Mechanical Sciences and Engineering*, Vol. 25, No. 3, July 2003, pp. 215–221.

[17] C. Genevois, A. Deschamps, and P. Vacher, "Comparative Study on Local and Global Mechanical Properties of 2024 T351, 2024 T6 and 5251 O Friction Stir Welds," *Materials Science and Engineering A*, Vol. 415, Nos. 1–2, 2006, pp. 162–170.

[18] Noyan, I. C., and Cohen, J. B., *Residual Stress Measurement by Diffraction and Interpretation*, Springer–Verlag, New York, 1987.

[19] Cullity, B. D., *Elements of X-Ray Diffraction*, 2nd ed., Addison Wesley Longman, Reading, MA, 1978.

[20] Jones, M. J., Heurtier, P., Desrayaud, C., Montheillet, F., Allehaux, D., and Driver, J. H., "Correlation Between Microstructure and Microhardness in a Friction Stir Welded 2024 Aluminium Alloy," *Scripta Materialia*, Vol. 52, No. 8, April 2005, pp. 693–697. doi:10.1016/j.scriptamat.2004.12.027

[21] Lemmen, H. J. K., Alderliesten, R. C., and Benedictus, R., "The Application of Finite Element Analyses for Fatigue Initiation and Crack Propagation in Friction Stir Welded Joints," *International Journal of Numerical Methods in Engineering* (to be published).

[22] Mishra, R. S., and Ma, Z. Y., "Friction Stir Welding and Processing," *Materials Science and Engineering R: Reports*, Vol. 50, Nos. 1–2, 2005, pp. 1–78.

[23] Norman, A. F., Brough, I., and Prangnell, P. B., "High Resolution EBSD Analysis of the Grain Structure in an AA2024 Friction Stir Weld," *Seventh International Conference ICCA7. Aluminium Alloys: Their Physical and Mechanical Properties*, Vol. 331–337, Trans Tech, Charlottesville, VA, 2000, pp. 1713–1718. doi:10.4028/www.scientific.net/MSF.331-337.1713

[24] Booth, D. P. P., Starink, M. J., and Sinclair, I., "Analysis of Local Microstructure and Hardness of 13 mm Gauge 2024-T351 AA Friction Stir Welds," *Materials Science and Technology*, Vol. 23, No. 3, 2007, pp. 276–284. doi:10.1179/174328407X157290

[25] Rajamanickam, N., Balusamy, V., Madhusudhanna Reddy, G., and Natarajan, K., "Effect of Process Parameters on Thermal History and Mechanical Properties of Friction Stir Welds," *Materials and Design*, Vol. 30, No. 7, 2009, pp. 2726–2731. doi:10.1016/j.matdes.2008.09.035

[26] Linton, V. M., and Ripley, M. I., "Influence of Time on Residual Stresses in Friction Stir Welds in Agehardenable 7xxx Aluminium Alloys," *Acta Materialia*, Vol. 56, No. 16, 2008, pp. 4319–4327. doi:10.1016/j.actamat.2008.04.059